Corrosion inhibition of N80 steel in simulated acidizing environment by *N*-(2-(2-pentadecyl-4,5-dihydro-1H-imidazol-1-YL) ethyl) palmitamide

Moses M. Solomon [a], Saviour A. Umoren [a,*], M.A. Quraishi [a], M.A. Jafar Mazumder [b]

[a] *Center of Research Excellence in Corrosion, Research Institute, King Fahd University of Petroleum and Minerals, Dhahran 31261, Saudi Arabia*
[b] *Chemistry Department, King Fahd University of Petroleum and Minerals, Dhahran-31261, Saudi Arabia*

ABSTRACT

A novel palmitic imidazoline compound, *N*-(2-(2-pentadecyl-4,5-dihydro-1H-imidazol-1-yl)ethyl)palmitamide (NIMP) has been successfully synthesized and characterized with Fourier transform spectroscopy (FTIR), Proton nuclear magnetic resonance (^{1}H NMR), and Carbon-13 nuclear magnetic resonance (^{13}C NMR). NIMP has been tested as corrosion inhibitor for N80 steel in 15% HCl solution at low and elevated temperatures using weight loss measurements, electrochemical impedance spectroscopy (EIS), potentiodynamic polarization (PDP), linear polarization (LPR), and electrochemical frequency modulation (EFM) techniques. The experimental investigation was supported with surface examination using scanning electron microscope (SEM), energy dispersive X-ray spectroscopy (EDAX), and Fourier transform spectroscopy (FTIR). NIMP is found to be effective in retarding N80 steel dissolution in 15% HCl solution at studied temperatures. The optimum concentration of NIMP is 300 ppm and this concentration afforded corrosion protection efficiency of 97.92% and 95.59% at 25 °C and 60 °C respectively from weight loss measurements. Chemisorption is proposed as the mechanism of adsorption of NIMP molecules onto N80 steel surface based on the value of standard enthalpy of adsorption (100.34 kJ/mol). PDP results disclosed that NIMP acted like a mixed type corrosion inhibitor but with principal effect on cathodic corrosion reactions. Surface screening results are in agreement with experimental results that NIMP molecules adsorbed on N80 steel surface. NIMP can be utilized as an acidizing corrosion inhibitor.

© 2018 Elsevier B.V. All rights reserved.

1. Introduction

The demand for effective and eco-friendly corrosion inhibitor that can withstand the severity of oil well acidizing is very high. The production of hydrocarbon can be reactivated in depleted wells by acidizing or reservoir fracture techniques [1–3]. This processes involve forcing acid solution (mostly HCl solution in the concentration range of 15–25% depending on whether the rock formation is made up of sandstone or limestone) down a well bore into formation rocks to etch it and create larger flow channels [1,2]. Production tubulars and well casings are mostly fabricated with low carbon steel. As the acid solutions move down to the rock formation, it contacts with metal structures and corrosion problem is created which eventually leads to failure. It is customary that the acid solution be fortified with corrosion inhibitors. Beside the high acid concentration, the temperature down well is very high. These harsh conditions make most common inhibitors to fail when utilized for well acidizing.

Generally, organic corrosion inhibitors are compounds containing heteroatoms like Nitrogen, Oxygen, Phosphorous, Sulphur, and/or

functionalities with pi electrons [4]. These heteroatoms and/or functional groups induce adsorption of organic molecules onto a metal surface by serving as the adsorption center. Organic nitrogenous compounds exhibit excellent capability towards metals corrosion mitigation. In fact, 90% of metals corrosion inhibitors in use currently are organic nitrogenous compounds basically long chain aliphatic diamines and imidazoles [5]. Compounds with imidazole/imidazoline ring are believed to involve in feedback coordinate covalent bonding with substrate surface easily during chemisorption process [6]. Numerous research works have therefore been devoted to this class of compounds. For example, Petrović Mihajlović et al. [7] studied the effects of imidazole and its structural derivatives namely purine, adenine and 6-benzylaminopurine on copper corrosion in seawater. It was found that the compounds behaved as typical mixed type corrosion inhibitor retarding both anodic and cathodic corrosion reactions. The inhibition efficiency of the compounds was found to follow the trend: imidazole > purine > adenine > 6-benzylaminopurine. Singh et al. [8] examined the corrosion inhibition performance of three imidazole derivatives namely 2-(4-methoxyphenyl)-4,5-diphenyl-imidazole (M-1), 4,5-diphenyl-2-(p-tolyl)-imidazole (M-2) and 2-(4-nitrophenyl)-4,5-diphenyl-imidazole (M-3) on J55 steel in sweet environment and found that M-1 exhibited the best inhibition efficiency of 93% at

* Corresponding author.
E-mail address: umoren@kfupm.edu.sa (S.A. Umoren).

400 mg/L concentration. Fouda et al. [9,10] found that, even at elevated temperatures, 1 mM *N*-(3-(dimethyl hexadecyl ammonio)propyl) palmitamide bromide and *N*-(3-(dimethyl octyl ammonio) propyl) palmitamide bromide could afford 98% protection to API N80 steel pipelines. In the investigation conducted by El-Haddad and Fouda [11], it was found that imidazole exhibited better corrosion inhibition for aluminium in HCl medium than methyl imidazole. *N*-(3-(dimethyl benzyl ammonio)propyl)lauramide chloride, *N*-(3-(dimethyl benzyl ammonio)propyl)myristamide chloride, and *N*-(3-(dimethyl benzyl ammonio)propyl)palmitamide chloride had equally been reported as effective corrosion inhibitor for mild carbon steel in acidic medium [12].

The corrosion inhibition by an organic compound is a complex phenomenon and inhibitive performance depends on variety of factors such as the chemical structure of the molecule, nature of substituents on the molecule, pH of corrosive environment, anions in corrosive medium, temperature, metallurgy, the charge on substrate surface, etc. Recently, Kovačević et al. [13] conducted an investigation into the role of different substituents namely, mercapto, benzene, and methyl groups on the corrosion inhibition of imidazoles. It was found that substituent has remarkable influence on adsorption cum corrosion inhibition of organic molecule. We pointed out in our review [14] that electron donating substituents enhance inhibition effectiveness while electron withdrawing substituents reduce corrosion inhibition potential of organic molecules. In this study, we examined the inhibitive efficacy of *N*-(2-(2-pentadecyl-4,5-dihydro-1H-imidazol-1-yl)ethyl)palmitamide (Scheme 1) (NIMP), a palmitic acid imidazoline in a simulated acidizing environment. The evaluation of the anticorrosive property of this compound was done using both chemical (weight loss measurements) and electrochemical (electrochemical impedance spectroscopy, potentiodynamic polarization, linear polarization resistance and electrochemical frequency modulation) methods and was supported with surface screening analysis with the aid of scanning electron microscope (SEM), energy dispersive X-ray spectroscopy (EDAX), and Fourier transform infrared spectroscopy (FTIR).

2. Experimental section

2.1. Chemicals

Diethylenediamine (99%), palmitic acid (≥99%), calcium oxide (≥99.99%), Ethyl acetate (99.8%) and HCl (37%) were purchased from Merck, USA.

2.2. Synthesis

The procedure reported by Bajpai and Tyagi [15] was followed for the synthesis of NIMP. In an open Pyrex vessel (500 mL), 2.06 g (20 mmol) of diethylenediamine, 10.25 g (40 mmol) of palmitic acid,

and 20 g of calcium oxide were carefully mixed. The reaction mixture was irradiated using a power of 850 W in a microwave oven for 7 min and the final temperature was noted. The reaction mixture was allowed to reach room temperature. Ethyl acetate was added (80 mL) and the mixture was heated until boiling and filtered off while hot, and the filtrate was concentrated under vacuum to dryness, 90.08% yield of a white to yellowish brown, solid to semisolid substance was obtained (Scheme 1).

2.3. Characterization of NIMP

The synthesized palmitic acid imidazole was characterized using FTIR, ^{1}H NMR and ^{13}C NMR. An FTIR (PerkinElmer Version 10.03.05 instrument) spectrometer was used for FTIR spectra recording. ^{1}H NMR and ^{13}C NMR characterization were achieved using a Bruker 500 MHz instrument operating at 500 MHz.
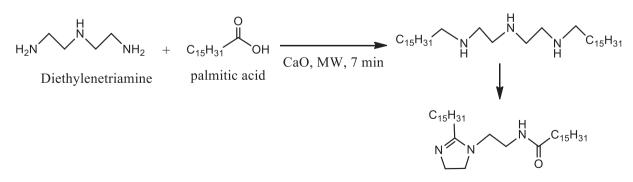
2.4. Anticorrosion studies

2.4.1. Specimens/solutions preparation

N80 steel grade with chemical composition (wt%) as follows: C 0.31; Si 0.19; Mn 0.92; P 0.010; S 0.008; Cr 0.2, balance Fe [16] was utilized in this study. For weight loss and electrochemical studies, the metal sheet was cut into coupons of 4 cm × 3 cm (surface area = 12 cm^2) and 2 cm × 2 cm respectively. The specimens for electrochemical studies were insulated using a Teflon tape such that the exposed area was 1 cm^2. The coupons were mechanically abraded using various grades of silicon carbide paper, specifically, #120, #320, #400, #600, and #800, sonicated in ethanol bath for 10 min so as to get rid of the dust emanating from the grinding process. Thereafter, they were degreased with ethanol and acetone, and finally dried in warm air [17]. The simulated acidizing medium was 15% HCl prepared by diluting 37% HCl (Analytical grade) with distilled water. The concentration ranges of *N*-(2-(2-pentadecyl-4,5-dihydro-1H-imidazol-1-yl)ethyl)palmitamide studied was 100–500 ppm by weight.

2.4.2. Weight loss measurements

Weight loss studies were done following the ASTM standard procedure [18]. The initial weight of the prepared N80 steel coupons were measured using a precision weighing scale balance. They were then immersed in different test solutions (blank and acid solutions containing 100, 200, 300, 400, and 500 ppm NIMP) and maintained at 25 °C and 60 °C, in a thermostated water bath for 6 h. After 6 h of immersion, the corroded coupons were removed, immersed in 1 M HCl for 20 s to soften the corrosion products, washed thoroughly in running water and distilled water, cleansed in acetone, and dried in a stream of warm air of about 40 °C. The dried coupons were reweighed to determine the weight loss (i.e. initial weight minus the final weight). The

Scheme 1. Synthesis route of *N*-(2-(2-pentadecyl-4,5-dihydro-1H-imidazol-1-yl)ethyl)palmitamide.

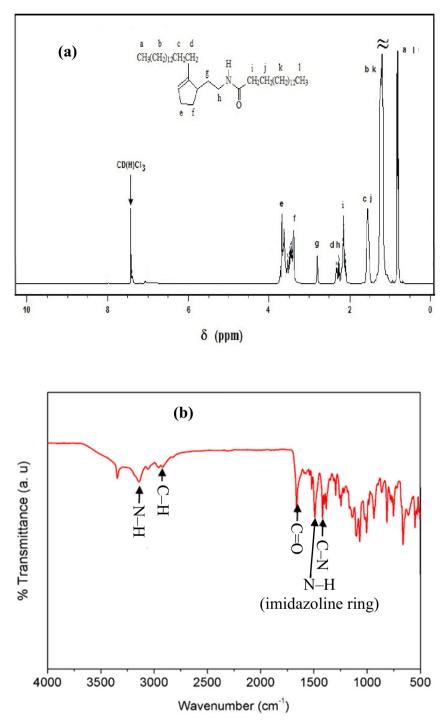**Fig. 1.** (a) ^{1}H NMR and (b) FTIR spectra of N-(2-(2-pentadecyl-4,5-dihydro-1H-imidazol-1-yl)ethyl)palmitamide.

corrosion rate (v) was computed using Eq. (1) [19]:

$$v(\text{mm per year}) = \frac{87.6 \times \Delta w}{\rho AT} \qquad (1)$$

where w = weigh loss (mg), ρ = density of the steel sample (g cm^{-3}), A = surface area of the specimen (cm^2), and T = immersion time (h). The inhibition efficiency (η) in percentage was calculated following Eq. (2):

$$\eta(\%) = \frac{v_{(\text{blank})} - v_{(\text{inh.})}}{v_{(\text{blank})}} \times 100 \qquad (2)$$

where $v_{(\text{blank})}$ and $v_{(\text{inh.})}$ are the corrosion rates in the absence and presence of NIMP respectively.

2.4.3. Electrochemical measurements

A Gamry Potentiostat/galvanost/ZRA (Ref 600) workstation was used for all electrochemical measurements. The instrument has EIS300, EFM140, and DC105 for impedance, frequency modulation, and polarization measurements respectively. The prepared N80 steel specimens were utilized as the working electrode, graphite rod as the counter electrode, and silver/silver chloride as the reference electrodes. Before the commencement of measurements, the working electrode was allowed in test solution for 3600 s so as to ensure a steady-state

Table 1
Calculated values of weight loss (mg), corrosion rate (mm per year), surface coverage (θ), and inhibition efficiency (η) for N80 steel in 15% HCl solution from weight loss measurements.

Concentration (ppm)	Weight loss (mg)		v (mm p y)		θ		η(%)	
	25 °C	60 °C	25 °C	60 °C	25 °C	60 °C	25 °C	60 °C
0	130.30	1660.60	20.20	257.05	–	–	–	–
100	3.80	296.90	0.59	45.96	0.97	0.82	97.08	82.12
200	2.90	138.30	0.45	21.41	0.98	0.92	97.77	91.67
300	2.70	73.20	0.42	11.33	0.98	0.96	97.92	95.59
400	3.50	86.90	0.54	13.45	0.97	0.95	97.33	94.77
500	3.30	92.70	0.51	14.35	0.97	0.94	97.48	94.42

open-circuit potential (OCP). Electrochemical impedance measurements were done between the frequency ranges of 100, 000 Hz to 0.01 Hz with amplitude of 10 mV peak to peak. For potentiodynamic polarization (PDP) studies, the working electrode was scanned at a rate of 0.2 mV/s relative to free corrosion potential (E_{corr}) from cathodic potential of −250 mV to anodic potential of +250 mV. To obtained polarization parameters, Tafel segments of measured polarization curves were extrapolated to corrosion potential. EFM measurements were performed using potential perturbation signal with amplitudes of 10 mV. Experiments were perform using two frequencies, 2 and 5 Hz. The base frequency was 1 Hz with 32 cycles so that the sinusoidal waveform repeats after 1 s [17]. Linear polarization resistance (LPR) measurements were done by polarizing the N80 steel electrode from −15 mV to +15 mV versus open-circuit potential at a sweep rate of 0.125 mV/s. The polarization resistance (R_p) was derived from the slope of the potential-current curve in the vicinity of E_{corr}. Inhibition efficiency (η) from electrochemical impedance spectroscopy (EIS), PDP, and LPR was computed using Eqs. (3), (4), and (5) respectively.

$$\eta_{EIS} = \left(1 - \frac{R^0}{R}\right) \times 100 \qquad (3)$$

$$\eta_{PDP} = \left(1 - \frac{i_{corr}}{i_{corr}^0}\right) \times 100 \qquad (4)$$

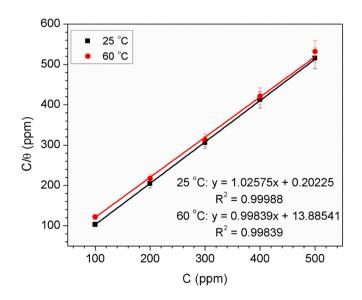$$\eta_{LPR} = \left(1 - \frac{R_p^0}{R_p}\right) \times 100 \qquad (5)$$

where $R^0, i_{corr}{}^0$, and R_p^0, are the charge transfer resistance, corrosion current density, and polarization resistance respectively in the absence of NIMP. R, i_{corr}, and R_p are the charge transfer resistance, corrosion current density, and polarization resistance respectively in the presence of NIMP.

2.4.4. Surface examination

The morphologies of the surfaces of N80 specimens immersed in 15% HCl solutions without and with NIMP for 24 h and the elemental composition of the corrosion products and/or adsorbed inhibitor films on the specimen surfaces were determined using a Scanning Electron Microscope (SEM) JEOL JSM-6610 LV coupled to energy dispersive X-ray spectroscopy (EDAX). The FTIR model given in Section 2.4 was also used for the characterization of films extracted from corroded samples surfaces.

3. Results and discussion

3.1. Findings from characterization

The molecular weight and melting point of *N*-(2-(2-pentadecyl-4,5-dihydro-1H-imidazol-1-yl)ethyl)palmitamide was found to be 561.97 g/mol and 62.9 °C respectively. Fig. 1 shows the ^{1}H NMR and FTIR spectra obtained for NIMP. The ^{1}H NMR (Fig. 1(a)) and ^{13}C NMR results confirmed the successful synthesis of NIMP. Found: (^{1}H NMR) CH₃ (0.86 ppm, 0.87 ppm, 0.89 ppm), (CH₂)n (1.25 ppm), CH₂ attached to imidazolium ring (2.66 ppm, 2.75 ppm, 2.80 ppm) –CONH- 6.1 ppm equivalent ring methylene group (3.34 ppm, 3.64 ppm). ^{13}C NMR: C₂ of imidazoline ring 118.8 ppm, equivalent ring of methyl carbon 49.4, equivalent methylene carbon 33.1 ppm, and CH₂ 29.5 ppm. In Fig. 1 (b), the stretching peak of C—H in CH₃ is found at 2951 cm⁻¹ and CH₂ skeletal band showed up at 719 cm⁻¹. Characteristic peaks of N—H (secondary amine), —C=O (amide), and C—N (imidazoline ring) stretching can be visibly seen at 3435 cm⁻¹, 1734 cm⁻¹, and 1655 cm⁻¹ respectively. The presence of these peaks in the spectrum reflects that NIMP was successfully synthesized.

3.2. Findings from anticorrosion property studies

3.2.1. Weight loss

In Table 1 is presented the weight loss, corrosion rate, surface coverage, and inhibition efficiency values derived from the weight loss experiments conducted to examine the effectiveness of NIMP as a corrosion inhibitor for N80 steel in 15% HCl solution. Judging from the results in the table, it could be said that NIMP is an effective inhibitor for steel in the considered environment. For instance, all the studied concentrations of NIMP reduced weight loss and corrosion rates of the metal samples by >80% at both low and elevated temperatures. In fact, inhibition efficiency is above 90% in all cases except 100 ppm at 60 °C. However, weight loss and corrosion rate values are higher at elevated temperature than at low temperature. This means that N80 steel is susceptible to rapid dissolution with increasing thermal agitation of aggressive solution [19]. A close inspection of the results in the table reveals that, weight loss and corrosion rate decreased while surface coverage and inhibition efficiency increased with increasing inhibitor concentration up to 300 ppm. After this concentration, the reverse is observed. It means, as the concentration of NIMP was increased, more of the molecules were available for adsorption and this led to greater surface coverage and in extension better inhibition performance. Beyond 300 ppm, the solution may have been saturated so that adsorbed inhibitor species began to interact with un-adsorbed species and as a consequent, some

Fig. 2. Langmuir adsorption isotherm plots at different temperatures for NIMP adsorption on N80 steel in 15% HCl.

Inside figure:
- 25 °C: y = 1.02575x + 0.20225, R² = 0.99988
- 60 °C: y = 0.99839x + 13.88541, R² = 0.99839
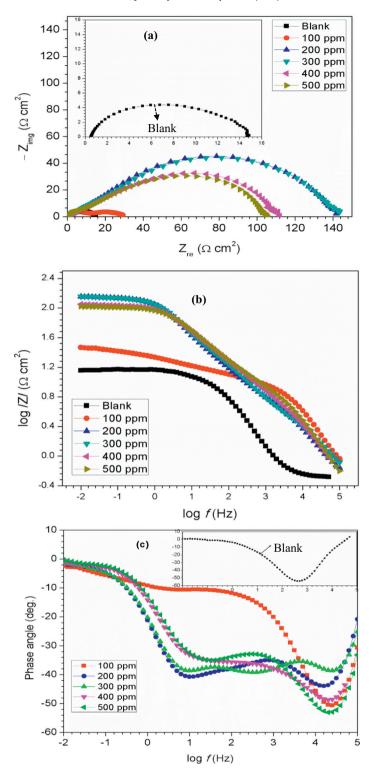- Axes: C/θ (ppm) vs C (ppm)

Fig. 3. Impedance plots for N80 steel in 15% HCl without and with different concentrations of NIMP exemplified as (a) Nyquist, (b) Bode modulus, and (c) Phase angle formats at 25 °C.

of the adsorbed films dissolved [19,20]. Therefore, 300 ppm is considered as the optimum concentration of NIMP. Also noticed in the table is the slight decrease in inhibition efficiency at elevated temperature. As it is known, temperature rise can cause desorption of adsorbed inhibitor films [21]. The optimum concentration afforded protective efficiency of 97.92% and 95.59% to N80 steel surface at 25 and 60 °C respectively.

Organic inhibitors retard metals dissolution by adsorption mechanism – a process of replacing adsorbed water molecules on a metal surface [22]. Inhibitor molecules perform this task via two approaches: physical interaction (interactions between charged substrate surface and inhibitor species [23]) and chemical interaction (donor – acceptor interaction [20]). Adsorption isotherms have proved useful in providing essential information on the interaction process between an inhibitor
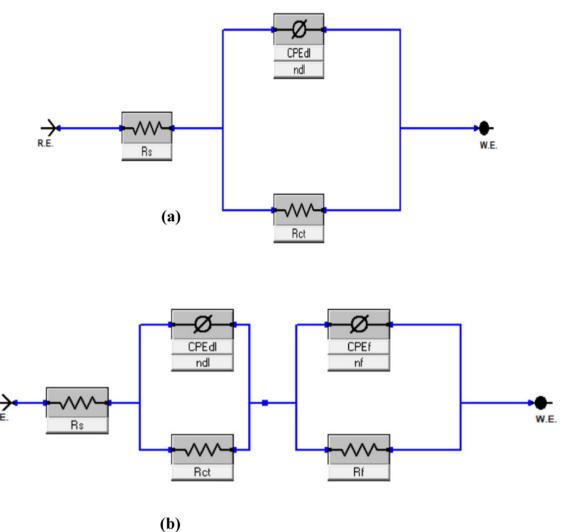
(a)

(b)

Fig. 4. Equivalent circuit diagrams used to fit impedance data in the (a) blank and (b) presence of NIMP.

and a metal surface [21,24,25]. Normally, experimental data are fitted into various adsorption isotherms and the best fit selected by making use of the linear regression coefficient (R^2). In an ideal situation, R^2 equals unity. In our case, the Langmuir adsorption isotherm is adopted because R^2 value and the slope are near unity (Fig. 2) in all cases. The Langmuir adsorption isotherm assumes the general form:

$$\frac{C_{inh}}{\theta} = \frac{1}{K_{ads}} + C_{inh} \qquad (6)$$

where θ is the surface coverage ($\theta = \eta/100$), K_{ads} is the equilibrium constant of the adsorption – desorption process, and C_{inh} is the concentration of NIMP. Fig. 2 depicts the linear graphs obtained for the

adsorption process of NIMP molecules onto N80 steel surface by plotting C_{inh}/θ as a function of C_{inh}. The K_{ads} defines the strength of the bond between an adsorbate and adsorbent [25]. High K_{ads} values indicates strong interaction. From the intercepts of the graphs in Fig. 2, K_{ads} values of 4.94 L mg^{-1} and 0.07 L mg^{-1} were deduced for the studied process at 25 °C and 60 °C respectively. The K_{ads} value was used in the computation of the standard free energy of adsorption (ΔG_{ads}^0) according to the following equation [26,27]:

$$\Delta G_{ads}^0 = -RT \, \ln\left(1 \times 10^6 K_{ads}\right) \qquad (7)$$

where 1×10^6 is the concentration of water molecules in mg/L or part

Table 2
Electrochemical impedance parameters for N80 steel in 15% HCl solution in the absence and presence of different concentrations of *N*-(2-(2-pentadecyl-4,5-dihydro-1H-imidazol-1-yl) ethyl)palmitamide at 25 °C.

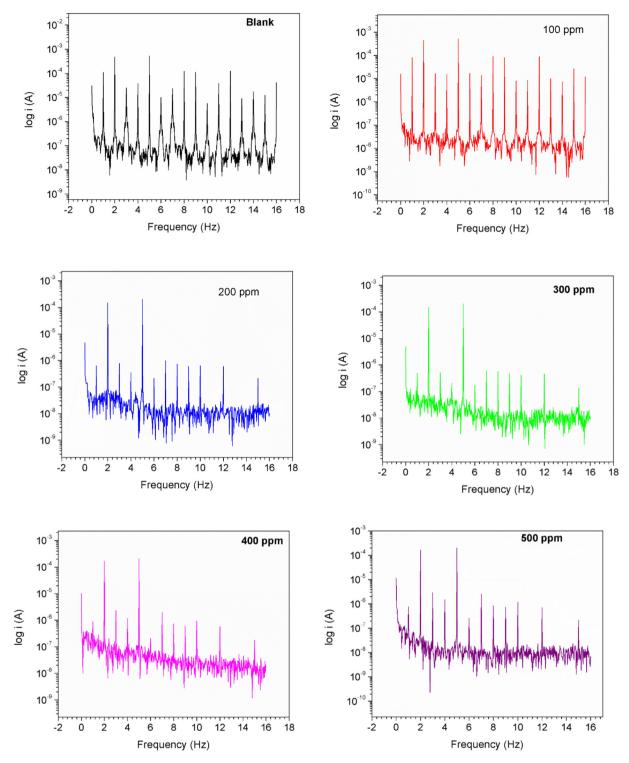| Conc. (ppm)	R_s (Ω cm^2)	CPE$_{dl}$ Y_{01} (mΩ^{-1} s^2 cm^{-2})	n_{dl}	R_{ct} (Ω cm^2)	CPE$_f$ Y_{02} (mΩ^{-1} s^2 cm^{-2})	n_f	R_f (Ω cm^2)	$R = R_{ct} + R_f$ (Ω cm^2)	C_{dl} (μF cm^{-2})	x^2 $\times 10^{-3}$	η_{EIS}
0	0.476	0.862	0.795	13.860	–	–	–	13.860	70.937	2.855	–
100	0.494	0.920	0.919	97.480	0.824	0.291	5.628	103.108	33.180	383.600	86.558
200	0.697	0.227	0.713	140.300	1.268	0.673	5.942	146.242	26.762	2.318	90.523
300	0.456	0.424	0.722	140.500	1.021	0.615	9.606	150.106	3.176	3.019	90.767
400	0.443	0.855	0.713	96.710	1.075	0.665	15.440	112.150	7.903	1.022	87.642
500	0.344	0.858	0.809	100.000	1.026	0.655	7.343	107.343	54.615	1.870	87.088

Fig. 5. Intermodulation spectra recorded for N80 steel in 15% HCl solution without inhibitor and with different concentrations of NIMP at 25 °C.

per million (same as concentration of inhibitor), R and T are the molar gas constant (8.3144598 J/K) and absolute temperature respectively. The calculated ΔG_{ads}^0 value at 25 °C and 60 °C are −38.19 kJ/mol and − 30.89 kJ/mol respectively. The values are negative and indicate that the adsorption of NIMP molecules onto the steel surface was spontaneous [26,27]. The standard enthalpy (ΔH_{ads}^0) for the adsorption process can be calculated from the famous can't Hoff equation given as:

$$\ln\left(\frac{K_{ads-2}}{K_{ads-1}}\right) = \frac{-\Delta H_{ads}^0}{R}\left(\frac{1}{T_2} - \frac{1}{T_1}\right) \qquad (8)$$

where K_{ads-2} and K_{ads-1} are the equilibrium adsorption constants at temperature T_2 (60 °C) and T_1 (25 °C) respectively. ΔH_{ads}^0 value obtained is 100.34 kJ/mol. The positive nature of this value implies that the adsorption process was endothermic [26]. In endothermic adsorption process, $\Delta H_{ads}^0 > 0$ signifies chemical adsorption whereas $\Delta H_{ads}^0 < 0$ indicates physical adsorption [26]. In our case, ΔH_{ads}^0 value is greater than zero meaning the adsorption of NIMP molecules onto N80 steel surface in 15% HCl solution was by chemisorption mechanism. This submission seems to be contrary to the deduction from the variation of inhibition efficiency with temperature (Table 1). As argued by some authors

Table 3

Electrochemical frequency modulation (EFM) parameters for N80 steel in 15% HCl solution in the absence and presence of different concentrations of N-(2-(2-pentadecyl-4,5-dihydro-1H-imidazol-1-yl)ethyl)palmitamide at 25 °C.

Conc. (ppm)	i_{corr} (μA cm^{-2})	β_a (mV dec^{-1})	β_c (mV dec^{-1})	CF–2	CF–3	η_{EFM} (%)
0	981.00	22.92	24.60	1.13	2.50	–
100	196.90	26.40	27.86	1.33	3.25	79.93
200	102.30	184.60	195.90	1.80	3.05	89.57
300	96.70	208.70	217.80	1.81	3.28	90.14
400	98.50	178.30	203.80	2.00	3.59	89.96
500	100.80	166.90	196.60	2.01	3.25	89.72

Table 4

Corrosion parameters for N80 steel in 15% HCl solution in the absence and presence of different concentrations of N-(2-(2-pentadecyl-4,5-dihydro-1H-imidazol-1-yl)ethyl) palmitamide at 25 °C from potentiodynamic polarization (PDP) and linear polarization resistance (LPR) methods.

Conc. (ppm)	PDP					LPR	
	$-E_{corr}$ (mV vs. Ag/AgCl)	i_{corr} (μA cm^{-2})	β_a (mV dec^{-1})	β_c (mV dec^{-1})	η_{PDP} (%)	R_p (Ω cm^2)	η_{LPR} (%)
0	500.00	894.0	94.10	138.70	–	13.39	–
100	475.00	122.30	80.70	87.90	86.32	91.14	85.30
200	527.00	95.30	152.50	152.20	89.34	147.40	90.92
300	533.00	87.80	166.60	192.50	90.18	151.10	91.14
400	523.00	98.10	80.20	166.60	89.03	115.30	88.39
500	526.00	102.10	104.00	80.20	88.58	108.50	87.66

[28–30], physisorption and chemisorption are not two independent mechanisms but one being a preceding step to another. Obviously, in a strong acid solution like the one considered in this study, NIMP would exist predominantly in protonated form. It has been reported that steel surface acquired net positive charge in 15% HCl solution and that chloride ions are specifically adsorbed on the surface [23,31,32]. Therefore, protonated NIMP molecules may have been electrostatically drag onto N80 steel surface as suggested by the variation of inhibition efficiency with temperature. However, on the surface, the adsorbed protonated molecules may have been freed such that the inhibitor molecules and the steel surface involve in a donor-acceptor interaction. The ═N—, N—C, and C═O as found in the NIMP molecule (Scheme 1) may have served as the sites for chemisorption [23]. Finally, the entropy of the adsorption (ΔS_{ads}^0) process was determined using Eq. (9) [26] and the value obtained is 0.209 J mol^{-1} K^{-1}. The positive ΔS_{ads}^0 value indicates a rise in the solvent energy during the adsorption process [26,33]. It also infers higher positive water desorption entropy [26,33]. According to Noor and Al-Moubaraki [34], the positive ΔS_{ads}^0 value is an indication that one molecule of inhibitor substituted more water molecules on the metal surface.

$$\Delta G_{ads}^0 = \Delta H_{ads}^0 + T\Delta S_{ads}^0 \qquad (9)$$

3.2.2. Electrochemical impedance spectroscopy (EIS)

Fig. 3 presents the electrochemical impedance spectra obtained for N80 steel in 15% HCl devoid of and containing different concentrations
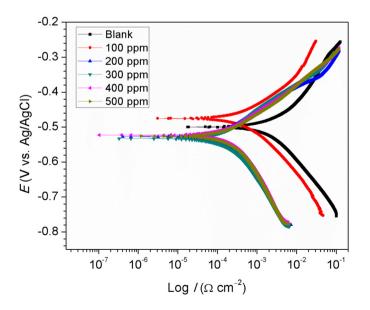

Fig. 6. Potentiodynamic polarization plots for N80 steel without and with different concentrations of NIMP at 25 °C.

of NIMP at 25 °C. In the impedance graph of uninhibited acid solution (Fig. 3(a)), a single capacitive loop is observed at high frequencies and this correspond to one time constant in the Bode representations (Fig. 3(b & c)). This loop represents the charge transfer resistance (R_{ct}) of the substrate in the studied acid solution [35,36]. In the Nyquist graphs drawn for inhibited systems, two semicircles are identified. The first is an unresolved semicircle between Z_{re} values of 0 and 12 Ω cm^2 while the second begins from Z_{re} value 12 Ω cm^2 and terminates at Z_{re} value 28, 108, 112, 140, and 144 Ω cm^2 for 100, 500, 400, 200, and 300 ppm respectively. These two semicircles correspond to two time constants noted in Fig. 3(b & c). They arose from the double layer structure of adsorbed NIMP film on the metal surface [37–39]. It suggests that the adsorbed NIMP film consist of two-layer structure: porous outer layer and compact inner layer [37–39]. The small unresolved semicircle could therefore denote the resistance of the outer layer while the large capacitive loop could represent the inner layer resistance [38,39]. However, all the Nyquist graphs are far from being perfect semicircles; a phenomenon often referred to as frequency dispersion [40] and arise due to heterogeneity of working electrode resulting from factors such as surface roughness, impurities, grain boundaries, dislocations, adsorption of inhibitors, etc. [40]. Compared with that of the uninhibited, the semicircles in the Nyquist graphs representing inhibited systems are larger in size; meaning that the adsorption of the inhibitor molecules on the metal surface makes charge transfer process difficult. The increment is however in this order: 300 ppm > 200 ppm > 400 ppm > 500 ppm > 100 ppm which is in excellent conformity with the weight loss results (Table 1), i.e. 300 ppm is the optimum concentration.

The selection of equivalent circuit (EC) for the fitting of the EIS data was guided by the features exhibited by the graphs in Fig. 3. A simple RQR equivalent circuit (Fig. 4(a)) with elements namely R_s (solution resistance), R_{ct} (charge transfer resistance), CPE_{dl} (constant phase element of inner layer) was selected for the fitting of the data recorded in uninhibited system. For the fitting of the data from inhibited systems, EC shown in Fig. 4(b) was used. CPE_f and R_f connote constant phase element and resistance of the outer layer of the adsorbed film respectively. The use of a CPE was necessary considering the imperfectness of the capacitive loop [37]. CPE can be described according to the following equation [41]:

$$Z_{CPE} = \frac{1}{Y_0(jw)^n} \qquad (10)$$

where Y_0 = modulus of the CPE, j = imaginary root ($j^2 = -1$), ω = angular frequency, and n = deviation parameter ($-1 \leq n \leq +1$) in terms of a phase shift. The CPE stand for a pure resistor when n = 0, an inductor when n = −1, Warburg impedance when n = 0.5, and a pure capacitor when n = +1 [37,41]. Good fits were obtained in all cases as evidence in the quite small values of chi square (Table 2) and associated errors that were <5%. All the electrochemical impedance parameters derived from the fitting process are given in Table 2. In the table, the values
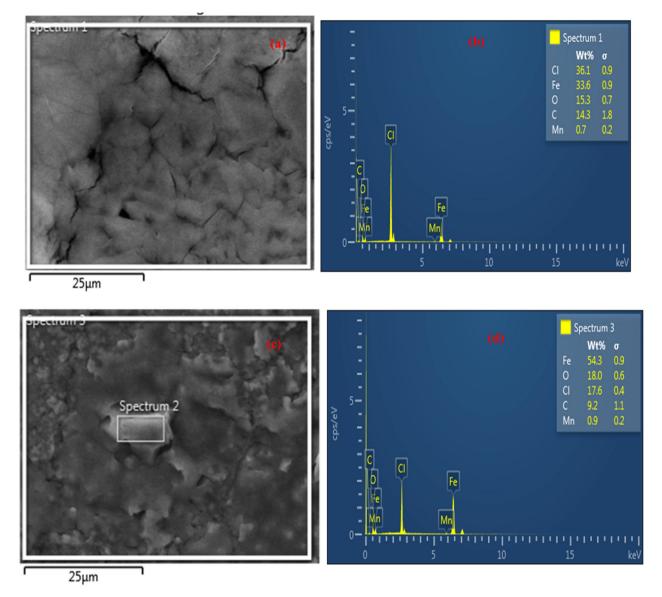
Fig. 7. SEM pictures and EDAX spectra for N80 steel after immersion in (a, b) 15% HCl solution, (c, d) 15% HCl solution containing 300 ppm NIMP at 25 °C for 24 h.
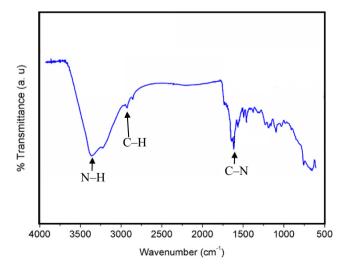

Fig. 8. FTIR spectrum of adsorbed film extracted from N80 steel surface after immersion in 15% HCl containing 300 ppm NIMP for 24 h at 25 °C.

of the double layer capacitance (C_{dl}) and inhibition efficiency (η) are also given. They were calculated using Eqs. (11) [42] and 3 respectively.

$$C_{dl} = \left(Y_{01} R_{ct}^{ndl-1} \right)^{1/ndl} \tag{11}$$

From the table, it is observed that R and η values increase while that of C_{dl} decrease as the concentration of NIMP was increased from 100 ppm to 300 ppm. The presence of 100 ppm NIMP raised R from 13.860 Ω cm^2 to 103.108 Ω cm^2 and reduced C_{dl} from 70.937 μF cm^{-2} to 33.180 70.937 μF cm^{-2}. By so doing, the metal specimen was protected by 86.558%. The R value further increased to 150.106 Ω cm^2 and C_{dl} dropped to 3.176 μF cm^{-2} upon increasing NIMP concentration to 300 ppm and the corresponding η is 90.767%. The observed increase in R value and decrease in C_{dl} value with increasing inhibitor concentration could be associated with larger surface coverage and increase in the thickness of adsorbed inhibitor film [43]. It is worthy to point out that the η of 200 ppm (90.523%) and 300 ppm (90.767%) is nearly the same meaning it would be profitable to utilize the 200 ppm concentration. Also worthy of mentioning is the fact that the N80 steel surface
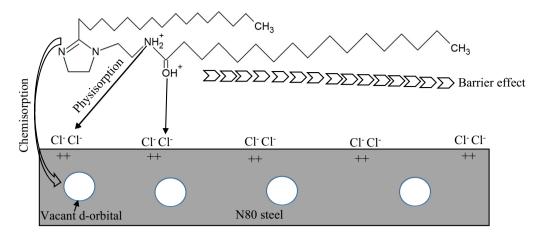
Fig. 9. Schematic illustration of the corrosion inhibition of N80 steel by NIMP in 15% HCl solution.

behaved as a capacitor in the studied medium, i.e., the n_{dl} values are close to one.

3.2.3. Electrochemical frequency intermodulation (EFM)

EFM was proposed by Bosch and Bogaerts [44] as a new electrochemical approach for monitoring online corrosion. One of the attractive features of this technique is the inherent data validation control using causality factor. For experimental results from EFM to be adjudged valid, the causality factor should not remarkably differ from their theoretical values. The theoretical value for causality factor 2 (CF-2) and 3 (CF-3) is 2 and 3 respectively [45]. Fig. 5 depicts the current response spectra recorded for N80 steel in 15% HCl without and with different concentrations of NIMP at 25 °C. In the spectra, two peaks are most prominent and are the response to the 2 Hz and 5 Hz excitation frequencies. Beside these bands, the other intense peaks are the harmonics, sums, and differences of the two excitation frequencies [46]. The less intense bands are noise signals. The prominent bands were used by the EFM 140 software package to compute the associated corrosion parameters namely, corrosion current density (i_{corr}), anodic and cathodic Tafel slopes (β_a & β_c), as well as the causality factors. The values of these parameters are listed in Table 3. Inhibition efficiency from this technique was calculated using Eq. (4). As could be seen in Table 3, the CF-2 and CF-3 values do not differ significantly from theoretical values hence this results should be valid. The i_{corr} value decrease in the presence of inhibitor and its variation with inhibitor concentration is as noted from weight loss (Table 1) and EIS (Table 2) results. The presence of NIMP cause both β_a & β_c to change but without a specific pattern on increasing NIMP concentration. This suggests that NIMP suppressed both the anodic and cathodic corrosion reactions. That is, NIMP behaved in the studied system as a mixed type corrosion inhibitor. The highest inhibition efficiency obtained from this technique is 90.14% afforded by the optimum concentration (300 ppm). The EFM and EIS results are in perfect agreement.

3.2.4. Potentiodynamic polarization (PDP) and linear polarization resistance (LPR)

Fig. 6 represents the influence of NIMP as inhibitor on the anodic and cathodic polarization characteristics of N80 steel in 15% HCl solution at 25 °C. By extrapolating the anodic and cathodic Tafel lines to corrosion potential (E_{corr}), the values of i_{corr}, β_a, and β_c were obtained and presented in Table 4. Eq. (4) was used for the calculation of inhibition efficiency. Inspection of Fig. 6 disclose that anodic and cathodic Tafel branches are shifted to lower current densities relative to that of the blank. This means that both anodic and cathodic corrosion reactions were retarded in the corrosive acid solution containing NIMP. It is however observed that the displacement is prominent on cathodic branches than anodic branches. The E_{corr} is seen to be shifted cathodically. These

observations infer that NIMP had greater inhibitive influence on the cathodic corrosion reactions than anodic half reactions [8]. The i_{corr}, β_a, and β_c values in Table 4 behave in like manner as those discussed under EFM (Table 3) with increasing inhibitor concentration. Again, the optimum concentration (300 ppm) offered the best inhibition efficiency of 90.18% which is in good agreement with results from EFM (Table 3), EIS (Table 2), and weight loss (Table 1).

The corrosion inhibition of N80 steel in 15% HCl solution without and with NIMP was also studied using linear polarization resistance technique and the values of polarization resistance (R_p) and η (calculated using Eq. (5)) are equally given in Table 4. The value of R_p and η increase with increasing inhibitor concentration up to 300 ppm and thereafter decrease. The optimum concentration raised the polarization resistance of the metal from 13.39 Ω cm^2 to 151.10 Ω cm^2 and the corresponding inhibition efficiency is 91.14%. The results from all the applied techniques (Table 1-4) portray NIMP as effective corrosion inhibitor for steel in acidizing environment.

3.3. Surface screening

To confirm the experimental results that NIMP molecules were adsorbed on N80 steel surface and protected it against corrosion in 15% HCl solution, surface examination was undertaken. In Fig. 7 is displayed the scanning electron microscope (SEM) pictures and energy dispersive X-ray spectroscopy (EDAX) spectra obtained for N80 specimens after immersion in 15% HCl (a, b) without and (c, d) containing 300 ppm NIMP for 24 h at 25 °C. The metal surface shown in Fig. 7 (a) is covered with corrosion products and the corresponding EDAX spectrum (Fig. 7(b)) disclose that the surface was rich in chloride ions. Compared with the image in Fig. 7(a), the products that covered the surface in Fig. 7(c) is more compact. The EDAX spectrum in Fig. 7(d) reveals that the chloride ions were less in the surface in Fig. 7(c) compared to the surface in Fig. 7(a). For instance, the wt% Cl is 36.1 in Fig. 7(b) and 17.6% in Fig. 7(d). Inhibitor molecules may have adsorbed on the surface and protected the surface against further dissolution.

To further proof the adsorption of NIMP molecules on N80 steel surface in the studied environment, a FTIR spectrum of extracted adsorbed film from N80 steel surface after immersion in 15% HCl containing 300 ppm NIMP for 24 h at 25 °C was obtained and is shown in Fig. 8. When comparing this spectrum with the FTIR spectrum of the pure NIMP (Fig. 1(a)), it is observed that the characteristic peaks of N—H, —C=O, and C—N stretching at 3435.6 cm^{-1}, 1734.5 cm^{-1}, and 1655.0 cm^{-1} respectively are affected by the interaction of the molecule with the metal surface. For instance, in Fig. 8, the C=O peak diminished completely. The N—H and C—N became more prominent and shifted to 3357.4 cm^{-1} and 1373.0 cm^{-1} respectively. This is a reflection of the

involvement of these heteroatoms in adsorption process. Similar submission can be found in the corrosion literature [37,47].

3.4. Mechanism of corrosion inhibition by NIMP

The general mechanism of steel corrosion in chloride containing environment summarized thus [48,49]:

$$Fe + Cl^- \leftrightarrow (FeCl^-)_{ads} \tag{12}$$

$$(FeCl^-)_{ads} \leftrightarrow (FeCl)_{ads} + e^- \tag{13}$$

$$(FeCl)_{ads} \rightarrow (FeCl^+) + e^- \tag{14}$$

$$(FeCl^+) \leftrightarrow Fe^{2+} + Cl^- \tag{15}$$

This reaction can be interrupted in the presence of inhibitor. Organic compounds with heteroatoms like N, O, S, P and/or pi electrons can interact with metal surface and retard corrosion [9,10,48]. NIMP has three possible adsorption centers, N, O, and the imidazoline ring (Scheme 1). In 15% HCl solution, the O and N heteroatoms in the palmitic acid pendant group of NIMP would unarguably be protonated. The cationic form of NIMP would interact physically with the steel surface as exemplified by Eq. (16).

$$(FeCl^-)_{ads} + NIMP^+ \rightarrow (FeCl^- NIMP^+)_{ads} \tag{16}$$

On the steel surface, electron pair from the imidazoline ring can be donated to the empty d-orbital of Fe resulting in covalent kind of bonding. Therefore, the adsorption of NIMP molecules on N80 steel surface in the studied acid environment involves both physisorption and chemisorption mechanisms. This proposition is strongly supported by the slight decline in inhibition efficiency (Table 1) and the ΔH_{ads}^0 value of 100.34 kJ/mol obtained in this study. Again, the large pendant group (i.e. palmitate) of NIMP could equally offer barrier effect on the metal surface. The high inhibition efficiency of NIMP obtained in this study is therefore attributed to the presence of many adsorption centers and large pendant group. The proposed mechanism is illustrated diagrammatically in Fig. 9.

4. Conclusion

On the basis of the findings from this investigation, the following conclusions are drawn:

1. *N*-(2-(2-pentadecyl-4,5-dihydro-1H-imidazol-1-yl)ethyl) palmitamide (NIMP) has been successfully synthesized from palmitic acid and diethylenetriamine. FTIR, ^{1}H NMR, and ^{13}C NMR characterization results confirmed the formation of NIMP.
2. NIMP is an effective corrosion inhibitor for N80 steel in 15% HCl solution both at low and elevated temperatures.
3. The optimum concentration of NIMP is 300 ppm. This concentration can afford corrosion protection efficiency of 97.48% and 94.42% at 25 °C and 60 °C respectively.
4. The mechanism of adsorption of NIMP molecules onto N80 steel surface is principally chemisorption as revealed by the value of standard enthalpy of adsorption (100.34 kJ/mol).
5. NIMP behaved like a mixed type corrosion inhibitor but its influence on cathodic corrosion half reactions is more than that on anodic half reactions.
6. Surface screening results provide evidence of the presence of NIMP molecules on N80 steel surface immersed in 15% HCl solution containing NIMP.

References

[1] L. Gandossi, An overview of hydraulic fracturing and other formation stimulation technologies for shale gas production, European Commission Joint Research Centre Technical Reports, 2013 https://doi.org/10.2790/99937.
[2] G. L. McClung IV. Acidizing materials and methods and fluids for earth formation protection. US 20130333892 A1, U.S. Patent 2013, Application No. 13/815,494.
[3] L. Kalfayan, Production Enhancement With Acid Stimulation, Pennwell Books, Tusla, Okla, 2008.
[4] S.A. Umoren, M.M. Solomon, Effect of halide ions on the corrosion inhibition efficiency of different organic species – a review, J. Ind. Eng. Chem. 21 (2015) 82.
[5] V.S. Sastri, Types of corrosion inhibitor for managing corrosion in underground pipelines, Underground Pipeline Corrosion 2014, pp. 166–211.
[6] M. Mousavi, M. Mohammadalizadeh, A. Khosravan, Theoretical investigation of corrosion inhibition effect of imidazole and its derivatives on mild steel using cluster model, Corros. Sci. 53 (2011) 3086.
[7] M.B. Petrović Mihajlović, M.B. Radovanović, Ž.Z. Tasić, M.M. Antonijević, Imidazole based compounds as copper corrosion inhibitors in seawater, J. Mol. Liq. 225 (2017) 127–136.
[8] A. Singh, K.R. Ansari, A. Kumar, W. Liu, C. Songsong, Y. Lin, Electrochemical, surface and quantum chemical studies of novel imidazole derivatives as corrosion inhibitors for J55 steel in sweet corrosive environment, J. Alloys Compd. 712 (2017) 121–133.
[9] A.S. Fouda, M.A. Elmorsi, T. Fayed, S.M. Shaban, O. Azazy, Corrosion inhibition of novel prepared cationic surfactants for API N80 carbon steel pipelines in oil industries, Surf. Eng. Appl. Electrochem. 54 (2) (2018) 180–193.
[10] A.S. Fouda, M.A. Elmorsi, Samy M. Shaban, T. Fayed, O. Azazy, Evaluation of *N*-(3-(dimethyl hexadecyl ammonio)propyl) palmitamide bromide as cationic surfactant corrosion inhibitor for API N80 steel in acidic environment, Egypt. J. Pet. (2017) https://doi.org/10.1016/j.ejpe.2017.10.004.
[11] M.N. El-Haddad, A.S. Fouda, Electroanalytical, quantum and surface characterization studies on imidazole derivatives as corrosion inhibitors for aluminum in acidic media, J. Mol. Liq. 209 (2015) 480–486.
[12] S.M. Shaban, *N*-(3-(dimethyl benzyl ammonio)propyl)alkanamide chloride derivatives as corrosion inhibitors for mild steel in 1 M HCl solution: experimental and theoretical investigation, RSC Adv. 6 (2016) 39784–39800.
[13] N. Kovačević, I. Milošev, A. Kokalj, The roles of mercapto, benzene, and methyl groups in the corrosion inhibition of imidazoles on copper: II. Inhibitor–copper bonding, Corros. Sci. 98 (2015) 457–470.
[14] C. Verma, L.O. Olasunkanmi, E.E. Ebenso, M.A. Quraishi, Substituents effect on corrosion inhibition performance of organic compounds in aggressive ionic solutions: a review, J. Mol. Liq. 251 (2018) 100–118.
[15] D. Bajpai, V.K. Tyagi, Microwave synthesis of cationic fatty imidazolines and their characterization, J. Surfactant Deterg. 11 (2008) 79–87.
[16] K.R. Ansari, M.A. Quraishi, A. Singh, Pyridine derivatives as corrosion inhibitors for N80 steel in 15% HCl: electrochemical, surface and quantum chemical studies, Measurement 76 (2015) 136–147.
[17] M.M. Solomon, S.A. Umoren, I.B. Obot, A.A. Sorour, H. Gerengi, Exploration of dextran for application as corrosion inhibitor for steel in strong acid environment: effect of molecular weight, modification, and temperature on efficiency, ACS Appl. Mater. Interfaces 10 (2018) 28112–28129.
[18] ASTM-G 01–03, ASTM Book of Standards, vol. 3, ASTM, West Conshohocken, 2003 02.
[19] M.T. Alhaffar, S.A. Umoren, I.B. Obot, S.A. Ali, Isoxazolidine derivatives as corrosion inhibitors for low carbon steel in HCl solution: experimental, theoretical and effect of KI studies, RSC Adv. 8 (2018) 1764–1777.
[20] M.K. Pavithra, T.V. Venkatesha, K. Vathsals, K.O. Nayana, Synergistic effect of halide ions on improving corrosion inhibition behaviour of benzisothiozole-3-piperizine hydrochloride on mild steel in 0.5M H$_2$SO$_4$ medium, Corros. Sci. 52 (2010) 3811–3819.
[21] Y. Tang, F. Zhang, S. Hu, Z. Cao, Z. Wu, W. Jing, Novel benzimidazole derivatives as corrosion inhibitors of mild steel in the acidic media. Part I: gravimetric, electrochemical, SEM and XPS studies, Corros. Sci. 74 (2013) 271–282.
[22] D. Gopi, E.M. Sherif, M. Surendiran, M. Jothi, P. Kumaradhas, L. Kavitha, Experimental and theoretical investigations on the inhibition of mild steel corrosion in the ground water medium using newly synthesized bipodal and tripodal imidazole derivatives, Mater. Chem. Phys. 147 (2014) 572–582.
[23] U. Eduok, E. Ohaeri, J. Szpunar, Electrochemical and surface analyses of X70 steel corrosion in simulated acid pickling medium: effect of poly (*N*-vinyl imidazole) grafted carboxymethyl chitosan additive, Electrochim. Acta 278 (2018) 302–312.
[24] D. Zhang, Y. Tang, S. Qi, D. Dong, H. Cang, G. Lu, The inhibition performance of long-chain alkyl-substituted benzimidazole derivatives for corrosion of mild steel in HCl, Corros. Sci. 102 (2016) 517–522.
[25] M.M. Solomon, S.A. Umoren, I.I. Udosoro, A.P. Udoh, Inhibitive and adsorption behaviour of carboxymethyl cellulose on mild steel corrosion in sulphuric acid solution, Corros. Sci. 52 (2010) 1317–1325.
[26] M.M. Solomon, H. Gerengi, S.A. Umoren, Carboxymethyl cellulose/silver nanoparticles composite: synthesis, characterization and application as a benign corrosion inhibitor for St37 steel in 15% H$_2$SO$_4$ medium, ACS Appl. Mater. Interfaces 9 (2017) 6376–6389.
[27] P. Roy, A. Pal, D. Sukul, Origin of the synergistic effect between polysaccharide and thiourea towards adsorption and corrosion inhibition for mild steel in sulphuric acid, RSC Adv. 4 (2014) 10607–10613.
[28] M.M. Solomon, S.A. Umoren, Performance evaluation of poly (methacrylic acid) as corrosion inhibitor in the presence of iodide ions for mild steel in H$_2$SO$_4$ solution, J. Adhes. Sci. Technol. 29 (11) (2015) 1060–1080.

[29] K. Ramya, R. Mohan, K.K. Anupama, A. Joseph, Electrochemical and theoretical studies on the synergistic interaction and corrosion inhibition of alkyl benzimidazoles and thiosemicarbazide pair on mild steel in hydrochloric acid, Mater. Chem. Phys. 149–150 (2015) 632–647.

[30] M. Mobin, M.A. Khan, Adsorption and corrosion inhibition behavior of polyethylene glycol and surfactants additives on mild steel in H_2SO_4, J. Mater. Eng. Perform. 23 (2014) 222–229.

[31] F. Bentiss, B. Mernari, M. Traisnel, H. Vezin, M. Lagrenee, On the relationship between corrosion inhibiting effect and molecular structure of 2,5-bis(npyridyl)-1,3,4-thiadiazole derivatives in acidic media: AC impedance and DFT studies, Corros. Sci. 53 (2011) 487–495.

[32] S.B. Jiang, L.H. Jiang, Z.Y. Wanga, M. Jin, S. Bai, S. Song, X. Yan, Deoxyribonucleic acid as an inhibitor for chloride-induced corrosion of reinforcing steel in simulated concrete pore solutions, Constr. Build. Mater. 150 (2017) 238–247.

[33] A.R. Hoseinzadeh, I. Danaee, M.H. Maddahy, M.R. Avei, Taurine as a green corrosion inhibitor for AISI 4130 steel alloy in hydrochloric acid solution, Chem. Eng. Commun. 201 (2014) 380–402.

[34] E.A. Noor, A.H. Al-Moubaraki, Corrosion behavior of mild steel in hydrochloric acid solutions, Int. J. Electrochem. Sci. 3 (2008) 806–818.

[35] S. Banerjee, V. Srivastava, M.M. Singh, Chemically modified natural polysaccharide as green corrosion inhibitor for mild steel in acidic medium, Corros. Sci. 59 (2012) 35–41.

[36] P. Roy, P. Karfa, U. Adhikari, D. Sukul, Corrosion inhibition of mild steel in acidic medium by polyacrylamide grafted guar gum with various grafting percentage: effect of intramolecular synergism, Corros. Sci. 88 (2014) 246–253.

[37] S.A. Haladu, S.A. Umoren, S.A. Ali, M.M. Solomon, A.I. Mohammed, Synthesis, characterization and electrochemical evaluation of anticorrosion property of a tetrapolymer for carbon steel in strong acid media, Chin. J. Chem. Eng. (2018) https://doi.org/10.1016/j.cjche.2018.07.015.

[38] Z.B. Wang, H.X. Hu, Y.G. Zheng, W. Ke, Y.X. Qiao, Comparison of the corrosion behavior of pure titanium and its alloys in fluoride-containing sulfuric acid, Corros. Sci. 103 (2016) 50–65.

[39] Z.B. Wang, H.X. Hu, Y.G. Zheng, Synergistic effects of fluoride and chloride on general corrosion behavior of AISI 316 stainless steel and pure titanium in H2SO4 solutions, Corros. Sci. 130 (2018) 203–217.

[40] R. Mohan, A. Joseph, Corrosion protection of mild steel in hydrochloric acid up to 313 K using propyl benzimidazole: electroanalytical, adsorption and quantum chemical studies, Egypt. J. Pet. 27 (2018) 11–20.

[41] A.S. Fouda, M.A. Ismail, A.S. Abousalem, G.Y. Elewady, Experimental and theoretical studies on corrosion inhibition of 4-amidinophenyl-2,2′-bifuran and its analogues in acidic media, RSC Adv. 7 (2017) 46414–46430.

[42] N. El Hamdani, R. Fdil, M. Tourabi, C. Jama, F. Bentiss, Alkaloids extract of *Retama monosperma* (L.) Boiss. seeds used as novel eco-friendly inhibitor for carbon steel corrosion in 1M HCl solution: electrochemical and surface studies, Appl. Surf. Sci. 357 (2015) 1294–1305.

[43] E. Gutiérrez, J.A. Rodríguez, J. Cruz-Borbolla, J.G. Alvarado-Rodríguez, P. Thangarasu, Development of a predictive model for corrosion inhibition of carbon steel by imidazole and benzimidazole derivatives, Corros. Sci. 108 (2016) 23–35.

[44] R.W. Bosch, W.F. Bogaerts, Instantaneous corrosion rate measurement with small-amplitude potential intermodulation techniques, Corrosion 52 (3) (1996) 204–212.

[45] I.B. Obot, I.B. Onyeachu, Electrochemical frequency modulation (EFM) technique: theory and recent practical applications in corrosion research, J. Mol. Liq. 249 (2018) 83–96.

[46] E. Kus, F. Mansfeld, An evaluation of the electrochemical frequency modulation (EFM) technique, Corros. Sci. 48 (2006) 965–979.

[47] P.E. Alvarez, M.V. Fiori-Bimbi, A. Neske, S.A. Brandán, C.A. Gervasi, *Rollinia occidentalis* extract as green corrosion inhibitor for carbon steel in HCl solution, J. Ind. Eng. Chem. 58 (2018) 92–99.

[48] X. Ma, X. Jiang, S. Xia, M. Shan, X. Li, L. Yu, Q. Tang, New corrosion inhibitor acrylamide methyl ether for mild steel in 1 M HCl, Appl. Surf. Sci. 371 (2016) 248–257.

[49] A. Yurt, A. Balaban, S.U. Kandemir, G. Bereket, B. Erk, Investigation on some Schiff bases as HCl corrosion inhibitors for carbon steel, Mater. Chem. Phys. 85 (2004) 420–426.